



Light-driven carbon dioxide reduction to methane by *Methanosarcina barkeri*-CdS biohybrid



Jie Ye^a, Jing Yu^a, Yiyun Zhang^a, Man Chen^a, Xing Liu^a, Shungui Zhou^{a,*}, Zhen He^{b,*}

^a Fujian Provincial Key Laboratory of Soil Environmental Health and Regulation, College of Resources and Environment, Fujian Agriculture and Forestry University, Fuzhou 350002, China

^b Department of Civil and Environmental Engineering, Virginia Polytechnic Institute and State University, Blacksburg, VA 24061, USA

ARTICLE INFO

Keywords:
Biohybrid catalyst
Photoelectron transfer
Carbon dioxide reduction
Membrane-bound proteins

ABSTRACT

Semi-artificial photosynthesis has emerged as a promising approach to convert carbon dioxide to value-added chemicals. Herein, direct CO₂-to-CH₄ conversion was realized by an innovative biohybrid consisting of semiconductor nanoparticles and non-phototrophic methanogens. The interaction between a model methanogen *Methanosarcina barkeri* and photoactive CdS nanoparticles achieved a CH₄ production rate of 0.19 μmol/h with a quantum efficiency of 0.34%, comparable to that of plants or algae. The *M. barkeri*-CdS biohybrid exhibited a higher electrical conductivity than *M. barkeri* only and generated photocurrent in response to irradiation. The simultaneous increase of *mcrA* gene copies by 151.4% illustrated the robustness of this *M. barkeri*-CdS biohybrid. Membrane-bound proteins were found to play a key role in the photoelectron transfer. The CO₂-to-CH₄ conversion was possibly conducted with photoelectrons from the e⁻-h⁺ separation via the H₂ases-mediated and cytochromes-mediated pathways. The findings encourage further exploration of the solar-driven self-replicating biocatalytic system to achieve CO₂-to-CH₄ conversion.

1. Introduction

The significant contribution of carbon dioxide (CO₂) to climate change is driving the efforts to capture and reduce CO₂ through innovative technologies [1]. Conversion of CO₂ to value-added chemical products, for example methane (CH₄) that is an energy carrier with the calorific value of 890 kJ/mol, is of strong interest to addressing the CO₂ issue. However, the direct CO₂-to-CH₄ conversion is a kinetically complex and energetically intensive process. The associated activation energy should be exactly orchestrated to the forward reaction during the multiple proton-coupled electron transfers. Although this process can be realized by catalytic reductions with various homogeneous and/or heterogeneous catalysts [2–4], the poor chemoselective conversion remains a great challenge [5]. The issue of selectivity might be addressed by using biocatalysts such as enzymes that are isolated from microorganisms or plants and are able to selectively catalyze CO₂ reduction with low energy barriers [6]. However, both the lack of self-replication ability and oxygen intolerance of enzymes have constrained their applications.

The whole-cell microorganisms such as methanogens have also been studied for the CO₂-to-CH₄ conversion and can be operated in a more complicated environment with less energy loss, compared to enzymes.

The source of electrons can strongly affect the CO₂-to-CH₄ conversion by methanogens [7]. The traditional chemical electron donors are effective at an expense of either high cost (e.g., formate and acetate) or limited mass transfer (e.g., low water solubility of hydrogen gas). Alternative electron sources such as photoelectrons triggered by solar energy are considered potentially cost-effective with substantial energetic advantages [8]. Recent progress has demonstrated that the direct contact between microorganisms and light-harvesting semiconductors (semi-artificial photosynthesis) could successfully leverage the board-band light efficiency of semiconductors and highly specific biological catalytic power in living microorganisms to realize both chemical conversion and contaminant degradation [9,10]. Particularly, the efficient conversion of CO₂ to multi-carbon compounds by the biohybrid system demonstrated its potential for CO₂ reduction [11]. This has inspired our exploration of the CO₂-to-CH₄ conversion through interactions between methanogens and a semiconductor, which provided a potential way for integration into existing infrastructure for the delivery and use of natural gas.

In this study, we have demonstrated for the first time that the reduction of CO₂ to CH₄ could be accomplished by a methanogen-semiconductor biohybrid. *Methanosarcina barkeri* was chosen as a model methanogen with highly-efficient metabolism for CO₂-to-CH₄

* Corresponding authors.

E-mail addresses: sgzhou@soil.gd.cn (S. Zhou), zhenhe@vt.edu (Z. He).

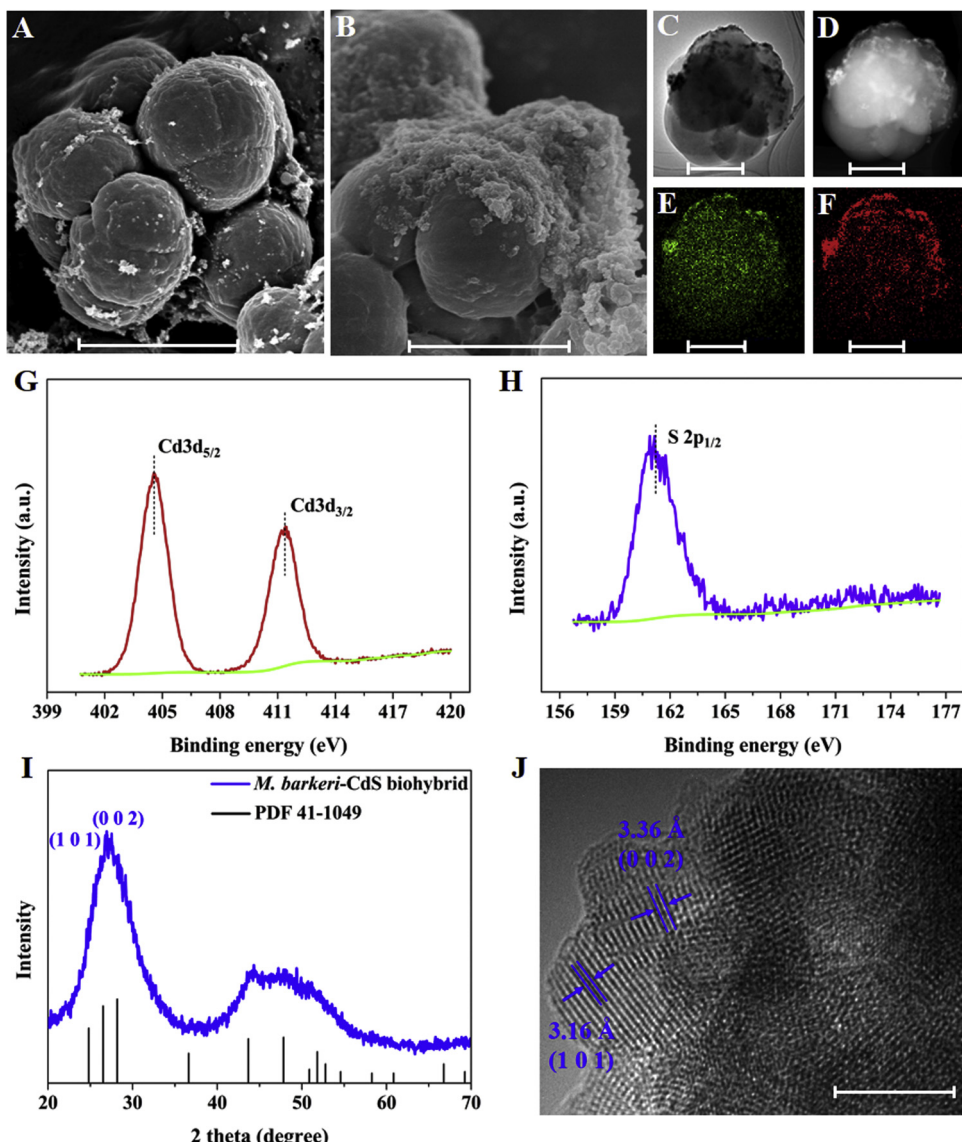


Fig. 1. Characterization of the *M. barkeri*-CdS biohybrid. Scanning electron microscopy (SEM) images of the *M. barkeri* (**A**) and *M. barkeri*-CdS biohybrid (**B**); TEM image of *M. barkeri*-CdS biohybrid (**C**); High-angle annular dark field (HAADF) image of the *M. barkeri*-CdS biohybrid (**D**) and elements formed by Cd (**E**) and S (**F**) by EDS mapping; high resolution XPS spectra of Cd 3d (**G**) and S 2p (**H**) for the *M. barkeri*-CdS biohybrid; XRD pattern (reference peak from JCPDS data card No. 41-1049) (**I**) and high resolution TEM image of the *M. barkeri*-CdS biohybrid (**J**). Scale bar(s) in (**A**, **B**) are 2 μm, in (**C-F**) are 1 μm, in (**J**) is 5 nm.

conversion [12]. Cadmium sulfide (CdS) nanoparticles were combination with *M. barkeri* as light-harvesters to construct the *M. barkeri*-CdS biohybrid. CdS nanoparticles are the promising quantum dots with the high absorption coefficient function as a photosensitizer, and their surface electrostatics can support the junction with methanogen to reduce the charge transfer barrier [13]. The synthesized *M. barkeri*-CdS biohybrid was characterized and its performance for the CO₂-to-CH₄ conversion was experimentally evaluated. The possible electron transfer mechanism under light irradiation was also analyzed and discussed. The results of this study expect to provide a novel insight for developing the self-augmented photo-biological system to accomplish the CO₂-to-CH₄ conversion.

2. Materials and methods

2.1. Synthesis of the *M. barkeri*-CdS biohybrid

M. barkeri MS (DSM 800) was purchased from DSMZ (Braunschweig, Germany). All culture and sampling manipulations

were performed in an anaerobic glovebox with a mixed gas atmosphere of 80% N₂ and 20% CO₂ (vol/vol). Primary cultures of *M. barkeri* were grown in a sterilized contained substrate medium (CSM) (Table S1) that was modified from DSM311b medium. Secondary cultures were started by diluting the late exponential phase primary cultures at a ratio of 1:5 into 50-mL sterilized CSM medium.

After 9–10 days of cultivation, the serum bottles with the CH₄ accumulation of 0.6 mmol were employed for the synthesis of the *M. barkeri*-CdS biohybrid (OD₆₀₀ ~ 0.2). The effect of different CdCl₂ concentrations (0.50, 0.75, 1.00, and 1.25 mM) on the performance of *M. barkeri*-CdS biohybrid was investigated by preliminary experiments, and the highest CH₄ yield was achieved with the concentration of 1.00 mM (Fig. S1). Therefore, a CdCl₂ concentration of 1.00 mM was used in this study (Fig. S2). After 3 days of cultivation, the color of the medium changed from white to yellow, indicating the formation of the *M. barkeri*-CdS biohybrid (Fig. S3). The suspension was then centrifuged at 5000 rpm for 10 min at 4 °C, and washed three times with 0.9% NaCl solution. The final pellets were resuspended with 0.9% NaCl solution (20 mL) and added into 125-mL serum bottles containing 50-mL

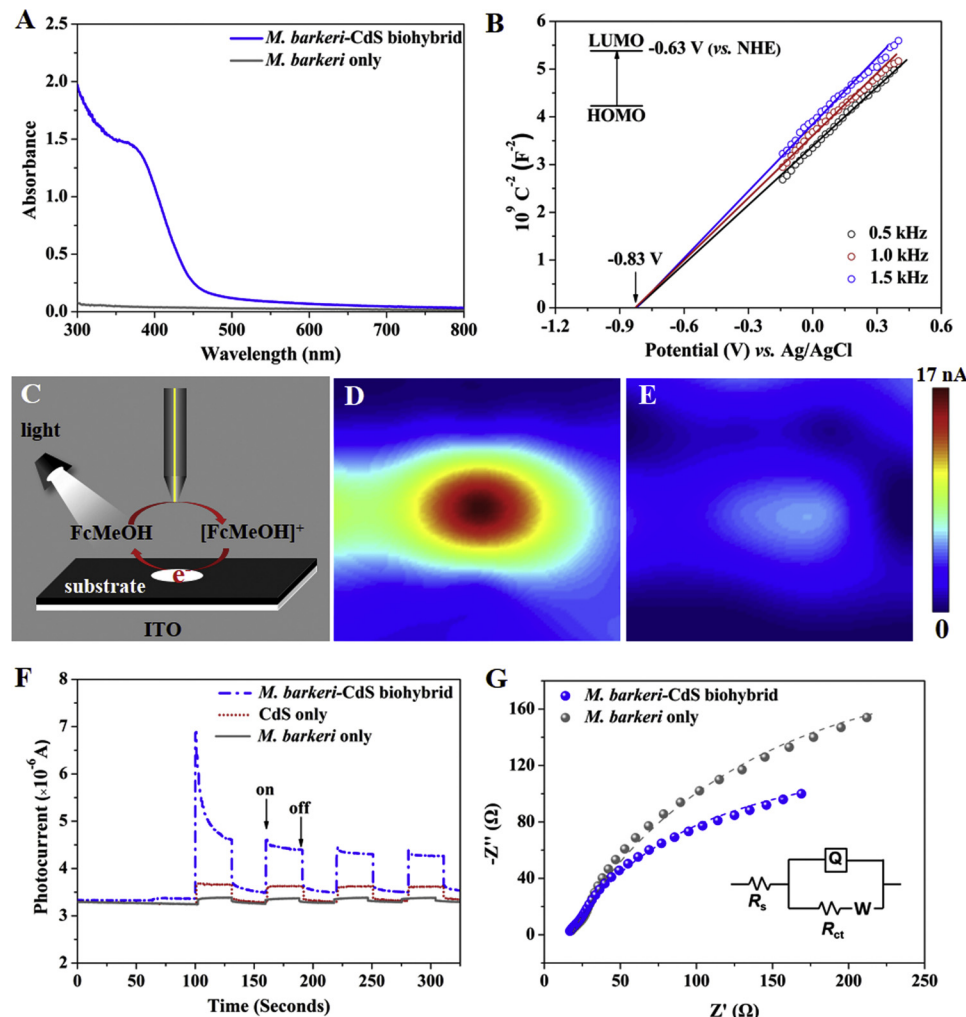


Fig. 2. Photoelectrochemical tests of the *M. barkeri*-CdS biohybrid. UV-vis spectrum (A) and Mott-Schottky plots (B) for the *M. barkeri*/*M. barkeri*-CdS biohybrid; schematic diagram of SECM imaging (C), and the measured tip photocurrent with the *M. Barkeri*-CdS biohybrid (D)/*M. Barkeri* (E) as substrate under light irradiation; *I-t* curves with a light on/off cycle (30/30 s) (F) and Nyquist plots (G) recorded from a three electrode electrochemical cell. LUMO: lowest unoccupied molecular orbital; HOMO: highest occupied molecular orbital.

sterilized uncontaminated substrate medium (USM) medium, in which NaAc and $\text{Na}_2\text{S}\cdot 9\text{H}_2\text{O}$ were removed (Table S1), and the suspension was sparged with sterile CO_2/N_2 (80/20, vol/vol). Cysteine (Cys) at 0.15 wt. % was selected as a sacrificial reducing agent to quench the hole pair [14]. The negligible CH_4 yield and decreased cell viability demonstrated that *M. barkeri* could not effectively use Cys as a potential carbon source for CH_4 production (Fig. S4).

2.2. Characterization of the *M. barkeri*-CdS biohybrid

The bare *M. barkeri* or *M. barkeri*-CdS biohybrid was fixed with 2.5% glutaraldehyde for 12 h, and dehydrated in 25%, 50%, 75%, 90% and 100% ethanol sequentially to observe the morphology. The suspensions were then dropped onto the silicon plate and dried at room temperature (ca. 25 °C). The platinum-sputtered samples (MC1000, Hitachi, Japan) were analyzed by a field-emission scanning electron microscopy (FESEM, SU8020, guolHitachi, Japan). The suspensions were also dropped onto a carbon film, dried at room temperature, and analyzed by field-emission transmission electron microscopy (FETEM, Tecnai G2 F20 S-TWIN, FEI, USA). The composition of surface elements was analyzed by an energy dispersive X-ray detector (X-MaxN, Oxford Instrument). The X-ray photoelectron spectroscopy (XPS) measurement was performed by a Thermo ESCALA 250 XPS spectrometer system using Al K α radiation with a 30 eV pass energy. The X-ray diffraction

(XRD) patterns of different samples were detected by using an X-ray diffractometer (XRD-6000, Shimadzu, Japan) with Cu K α radiation at 40 kV and 30 mA and recorded in a 2θ range of 20–70° at a scan speed range of 1°/min.

The ultraviolet-visible (UV-vis) spectra of the *M. barkeri*-CdS biohybrid suspensions were scanned by a UV spectrometer with an integrating sphere (UV2600, Shimadzu, Japan). The Mott-Schottky analyses of the *M. barkeri*-CdS biohybrid were conducted on a CHI 660 electrochemical workstation (CH Instruments Inc, Austin, TX) at a frequency of 0.5, 1.0 and 1.5 kHz. Scanning electrochemical microscopy (SECM) spectra of different samples were obtained with a VersaSCAN SECM instrument (AMETEK Inc., Berwyn, USA), in which an indium tin oxide (ITO) slide was covered by a light mask to improve the signal/noise ratio with a substrate area of 1 mm × 1 mm [15]. A 25-μm-diameter Pt microelectrode was chosen as the SECM tip ($E_{\text{probe}} = 0.3 \text{ V}$ vs Ag/AgCl), and the electrolyte was composed of 1 mM FcMeOH in 0.1 M KCl. The charge separation and the transfer resistance of the *M. barkeri*-CdS biohybrid were measured by the photocurrent (*I-t*) and electrochemical impedance spectroscopy (EIS) using a CHI-660E electrochemical workstation (CH Instruments Inc, Austin, TX). An ITO conductive glass slide (1 cm × 1 cm, ITO-*M. barkeri*/*M. barkeri*-CdS biohybrid) was used as the working electrode, and a platinum sheet and a saturated calomel electrode were employed as counter and reference electrodes, respectively. The thin film working electrodes were

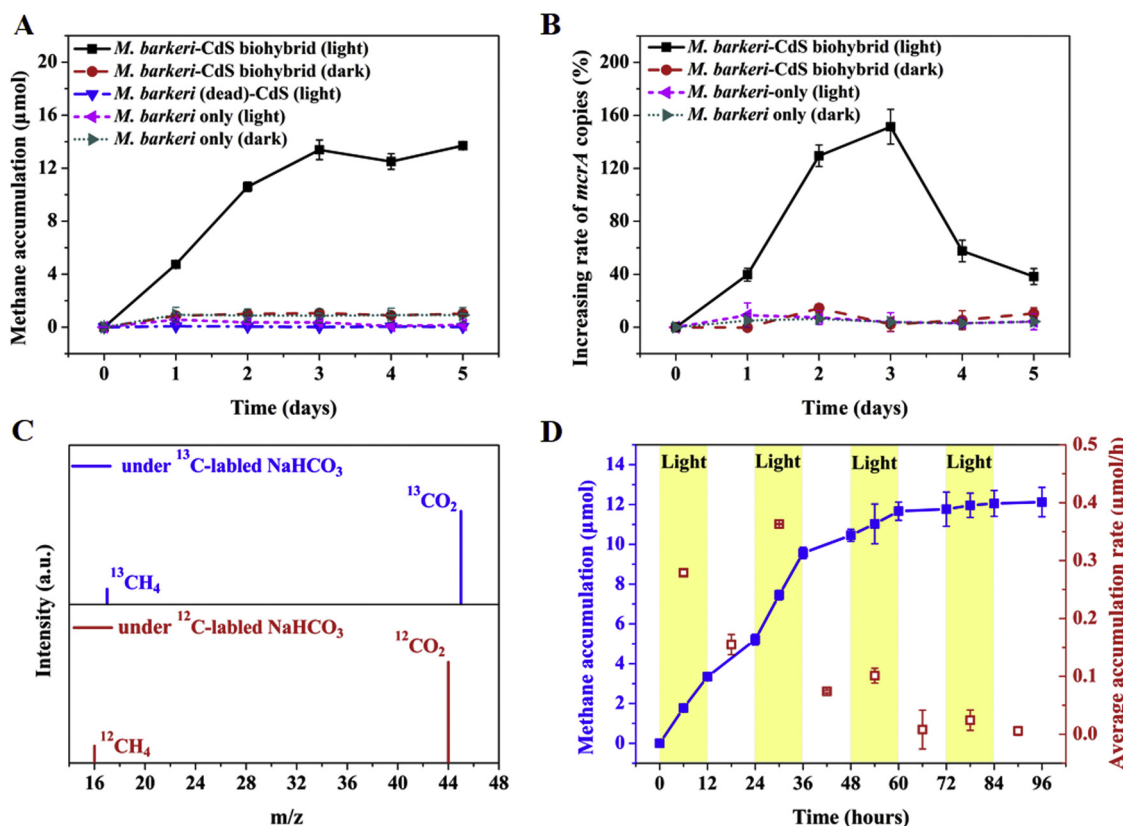


Fig. 3. The potential of *M. barkeri*-CdS biohybrid for the CO_2 -to- CH_4 conversion. Time curves of CH_4 accumulation (A) and the increasing rate of *mcrA* copies (B) by the *M. barkeri*-CdS biohybrid and deletional controls; mass spectrometry of headspace gases under the ^{12}C -labeled NaHCO_3 and ^{13}C -labeled NaHCO_3 in the media (C); CH_4 accumulation and average CH_4 accumulation rate by the *M. barkeri*-CdS biohybrid with a light-dark cycles of 12 h (D).

prepared by repeatedly drop-casting 5 μL suspensions onto ITO glass substrates followed by drying the film in air for 30 min (totally 50 μL for 10 times). A 0.1 M phosphate buffer solution (PBS) ($\text{pH} = 7$) with 0.1 M KCl aqueous solution was used as the electrolyte. PBS was prepared from NaH_2PO_4 and Na_2HPO_4 .

2.3. Light-driven CO_2 reduction experiments

The performance of the *M. barkeri*-CdS biohybrid for the CO_2 -to- CH_4 conversion was investigated under 395 ± 5 nm violet LEDs irradiation ($1.0 \pm 0.14 \text{ mW/cm}^2$) or a 300 W Xenon lamp (CEL-HXF300, Ceaulight, Beijing, China) with a 400 nm UV-cut filter. The light intensities were measured and calibrated by a light density meter (CEL-NP2000-2, Ceaulight, Beijing, China). In the control experiments, the effects of *M. barkeri*, CdS, and light were investigated. All experiments were conducted at 37°C with a constant temperature incubator.

To examine the source of the produced CH_4 , NaHCO_3 in the sterilized USM medium was substituted by ^{13}C -labeled NaHCO_3 . Then the produced $^{13}\text{CH}_4$ in headspace at each timepoint was measured with a gas chromatography-mass spectrometer (GC-MS, 7890-5975c, Agilent, USA) in the selected ion monitoring (SIM) ($m/z = 31, 46$) mode. The detailed GC-MS protocol was provided in the Supporting information. Meanwhile, as an indicator of the intracellular redox potential, nicotinamide adenine dinucleotide (NADH)/NAD ratio was measured by using NADH/NAD quantification kit (MAK 037, Sigma-Aldrich) to evaluate the change of reducing equivalent in cells during the biological CO_2 -to- CH_4 conversion.

For the proteinase K treatment, the *M. barkeri*-CdS biohybrid was incubated with 1.0–5.0 U/mL proteinase K for 1 h to digest the outer membrane proteins. Then, 5 mM proteinase inhibitor-phencylmethylsulfonyl fluoride (PMSF) was added to stop the proteolytic reaction. To further inactivate the activity of residual proteinase K, the

treated *M. barkeri*-CdS biohybrid was washed twice with 10 mM HEPES buffer solution containing PMSF. BacLight RedoxSensor Green Vitality Kit (Invitrogen Co.) was used to analyze the microbial vitalities before and after proteinase K treatment. The viabilities of *M. barkeri* were also evaluated using BacLight Live/Dead kit (Molecular Probes, Life Technologies, Germany) [16–18].

2.4. RNA collection and quantitative RT-PCR quantification

Cells were collected at early mid-log phase. The total RNA was extracted and purified using RNeasy Mini kits (Qiagen Inc., Valencia, CA, USA). The contaminated genomic DNA was further digested by DNase following the manufacturer's instruction (TURBO DNA-free Kit, ThermoFisher Scientific, Waltham, MA, USA). The final pure total RNA was reverse-transcribed into cDNA with random primers using the TransScript First-Strand cDNA Synthesis SuperMix (TransGen Biotech, Beijing, China). Briefly, 300 ng of total RNA was mixed with 0.1 μg random primer, 10 μL 2 \times TS Reaction Mix, 1 μL TransScript RT/RI Enzyme Mix, and the final volume was adjusted to 20 μL with nuclease-free water; the mixture was incubated at 25°C for 10 min, then 42°C for 15 min and finally heated at 85°C for 5 s to denature the enzyme. Quantitative PCR was carried out with a LightCycler 480 System (Roche, Penzberg, Germany). Primers targeting the genes encoding Ech, Vht, Hdr complex, *mcrA* and the housekeeping gene *rpoA1* were designed from the *M. barkeri* strain MS (Table S2). All primers were verified by PCR. Reaction were performed in quadruplicate for each gene tested in a total volume of 25 μL containing 12.5 μL of iTaq Universal SYBR Green Supermix (Biorad, Hercules, CA, USA), 0.6 mM of gene specific primers and 50 ng of cDNA. The real-time PCR was run for 40 cycles using 60°C as the annealing temperature.

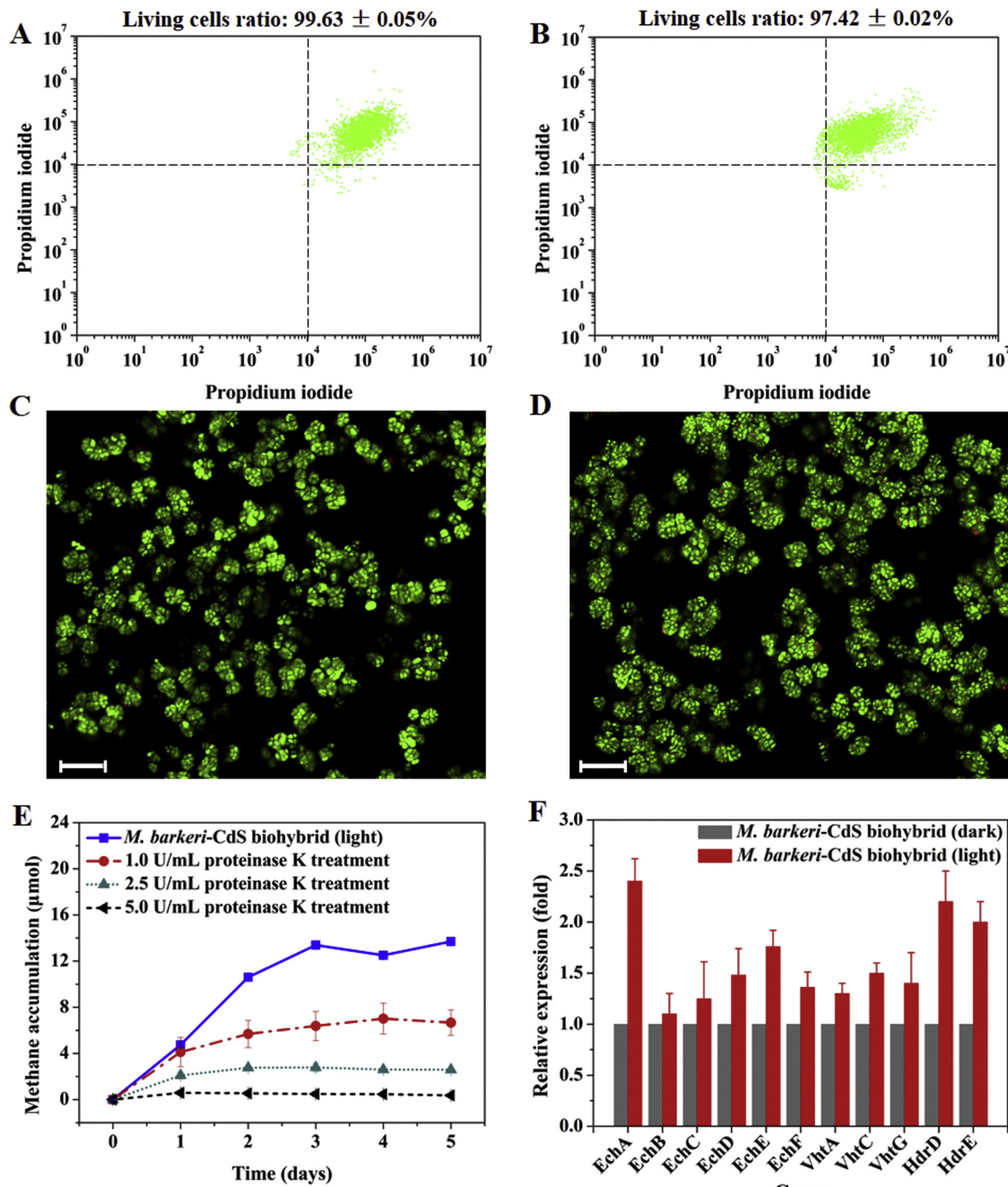


Fig. 4. Integrity test of *M. barkeri* cells and their effect on CH_4 production. Flow cytometry of *M. barkeri* before (A) and after (B) 5.0 U/mL proteinase K treatment with Redox Sensor Green reagent; LIVE/DEAD staining of *M. barkeri* before (C) and after (D) 5.0 U/mL proteinase K treatment; Time curves of CH_4 accumulation by the *M. barkeri*-CdS biohybrid under different doses (1.0, 2.5, 5.0 U/mL) of proteinase K treatment (E); Influence of light irradiation on expression of Ech, Vht and Hdr in the *M. barkeri*-CdS biohybrid (F). Scale bars in (C, D) are 10 μm (For interpretation of the references to colour in this figure legend, the reader is referred to the web version of this article).

2.5. Analytical methods

The produced CH_4 was measured by using an Agilent 7890A gas chromatograph (GC) equipped with a HP-5 column (30 m \times 0.32 mm) and flame ionization detector (FID). The specific conditions for GC were described in the Supporting information. Effects of light intensity on the CH_4 accumulation and average quantum yield (QE) by the *M. barkeri*-CdS biohybrid were evaluated based on the results of first 72 h irradiation under $395 \pm 5 \text{ nm}$ (λ) LED lamp (0.5, 1.0 mW/cm 2) or xenon lamp (2.0, 4.0, 8.0 mW/cm 2) with the irradiation area (A) of 37.5 cm 2 . The QE was calculated by the following equation:

$$\begin{aligned} \text{QE} &= \frac{\text{the number of electrons accepted by } \text{CO}_2}{\text{the number of incident photons}} \\ &\times 100\% = \frac{[8 \times C(\text{CH}_4)] \times 6.02 \times 10^{23}}{P_{\text{lightAt}t} / hc} \times 100\% \end{aligned} \quad (1)$$

where $C(\text{CH}_4)$, t , h , c was the CH_4 yield from hybrid system, reaction time, Planck constant ($6.63 \times 10^{-34} \text{ J/s}$) and speed of light ($3 \times 10^{17} \text{ nm/s}$), respectively.

All experiments were conducted in triplicate. Differences were evaluated using student's t test, and a p value < 0.05 was considered statistically significant.

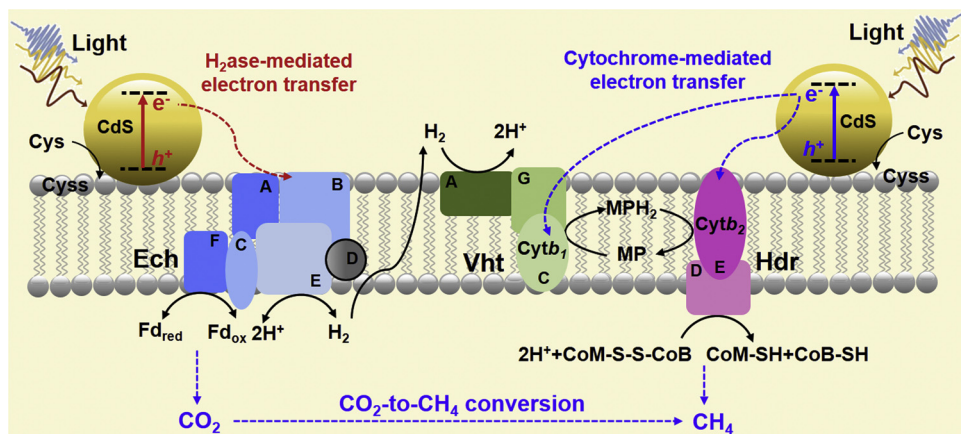


Fig. 5. Proposed photoelectrons transfer mechanism in the *M. barkeri*-CdS biohybrid.

3. Results and discussion

3.1. Characterization of the *M. barkeri*-CdS biohybrid

The synthesis of the *M. barkeri*-CdS biohybrid was indicated by the medium colour change to bright yellow (Fig. S3). Compared with *M. barkeri* only (Fig. 1A), a rougher surface was observed in the *M. barkeri*-CdS biohybrid (Fig. 1B). Transmission electron microscope (TEM) image and energy dispersive X-ray spectroscopy (EDS) mapping revealed that the particles distributed on the surface of *M. barkeri* had the diameters of 10–100 nm (Fig. 1C), and were mainly composed of cadmium (Cd) and sulfur (S) (Fig. 1D, E, F), demonstrating the successful formation of CdS nanoparticles on the microbial cells. Fig. 1G and 1H displayed the high-resolution XPS spectra of the Cd 3d and S 2p regions in the *M. barkeri*-CdS biohybrid. The peaks of Cd 3d_{5/2} at 404.6 eV and Cd 3d_{3/2} at 411.4 eV were associated with Cd²⁺ species [19], while the peak of S 2p_{3/2} at 161.2 eV was assigned to S²⁻ species [20,21]. The atomic ratio of Cd/S was approximately 1:1, thereby confirming the formation of CdS. This was further corroborated by XRD spectra (Fig. 1I) and high resolution TEM image (Fig. 1J), in which the crystalline CdS was identified (PDF 41-1049). The broad peaks on the XRD spectra were possibly due to the small size of the CdS nanoparticles [22].

UV-vis spectrum of the *M. barkeri*-CdS biohybrid yielded a measured direct band gap (E_g) of 2.69 eV ($\lambda_{\text{adsorption}} = 461 \text{ nm}$) (Fig. 2A), larger than that of the bulk CdS (2.42 eV); this may be attributed to the quantum confinement of small nanoparticles [23]. As shown in Fig. 2B, the slopes of Mott-Schottky plots were positive at different frequencies (0.5, 1.0, 1.5 kHz), indicating that the prepared CdS was an n-type characteristic semiconductor. The lowest unoccupied molecular orbital (LUMO) of the prepared CdS nanoparticles was -0.83 V vs Ag/AgCl (-0.63 V vs. NHE), which met the thermodynamical requirement for CO₂ reduction to CH₄ [24]. To understand the separation properties of photogenerated electron-hole pairs in the *M. barkeri*-CdS biohybrid, SECM tests were conducted (Fig. 2C). Negligible photocurrent was observed when *M. barkeri* or the *M. barkeri*-CdS biohybrid was scanned by SECM in the absence of irradiation (data no shown), revealing their insulating characteristics. In contrast, irradiation effectively triggered the photocurrent increase with the *M. barkeri*-CdS biohybrid (maximum 16.8 μA) (Fig. 2D), which was much higher than that with *M. barkeri* only under irradiation (Fig. 2E). During the intermittent on-off irradiation cycles, amperometric $I-t$ curves showed an immediate increase of photocurrent after the illumination of CdS, which was then declined upon the cease of the irradiation. In contrast, the photocurrent of *M. barkeri*-CdS biohybrid was higher than that of bare CdS (Fig. 2F). It might be due to the existence of membrane-bound e⁻ acceptors in *M. barkeri*, which was beneficial for electron transfer [25], and

subsequently suppressed the recombination of photo-electron and photo-hole pairs. Those results have demonstrated the quick transition of photoelectrons from valence band to conduction band in the *M. barkeri*-CdS biohybrid. EIS experiments were further conducted to investigate the photogenerated electron transfer efficiency at the interface. The EIS Nyquist plots were fitted by using ZSimpWin software to an equivalent circuit that comprised of solution resistance (R_s), the resistance for charge transfer cross the interface (R_{ct}), space charge capacitance (Q), and Warburg impedance (W). The interfacial resistance R_{ct} decreased from 441.5 (*M. Barkeri*) to 260.2 Ω (*M. barkeri*-CdS biohybrid), confirming the higher electronic conductivity of the *M. barkeri*-CdS biohybrid under irradiation (Fig. 2G).

3.2. *M. barkeri*-CdS biohybrid triggered the CO₂-to-CH₄ conversion

As shown in Fig. 3A, the production of CH₄ with the *M. barkeri*-CdS biohybrid increased to $13.70 \pm 0.01 \mu\text{mol}$ after 3-day irradiation, along with the 151.4% increase of the alpha subunit of methyl coenzyme M reductase gene copies (encoded by *mcrA*) (Fig. 3B). The *mcrA* gene was reported to determine the terminal step of CH₄ generation ($\text{Methyl-SCoM} + \text{CoBSH} \rightarrow \text{CH}_4 + \text{CoBS-SCoM}, \Delta G' = -30 \text{ kJ/mol}$) [15], and this was unique and ubiquitous to methanogens. The link between *mcrA* gene copy number and specific methanogenic activity (CH₄ flux) has also been demonstrated previously [26]. More *mcrA* gene copies in the *M. barkeri*-CdS biohybrid under light irradiation indicated the higher methanogenic activities and abundance. This was because that the photoelectron e⁻ excited from CdS could be injected to a membrane-bound e⁻ acceptor (such as cytochrome b) or membrane-bound H₂ase (such as Ech) of *M. barkeri* (demonstrated in the following part). Then, the additional electron donors would promote the generation of the proton motive force for ATP synthesis and high energy reducing equivalents such as H₂. Such accelerated methanogenesis by *M. barkeri* would lead to the increase of *mcrA* gene copies for the reduction of methyl-coenzyme M and CH₄ release.

A series of control experiments in which *M. barkeri*, CdS, and light were systematically removed, were conducted to further verify the photosynthesis of the *M. barkeri*-CdS biohybrid. As shown in Fig. 3A, a small amount of CH₄ (about 1.0 μmol) was produced in the first 24 h with *M. barkeri* only (dark), possibly due to the residual acetate or metabolic intermediates during the culture of *M. barkeri* with CSM medium. In contrast, negligible CH₄ production was observed with *M. barkeri* only under light irradiation. *M. barkeri* was reported to be photosensitive to light irradiation [27]; as a result, the harmful effect from the light might interfere with the normal physiological metabolism for CH₄ production. This was supported by the fact that the copies of *mcrA* gene did not increase with *M. barkeri* only (Fig. 3B), suggesting the inhibition of cell viability. SEM images also revealed the obvious

cell shrinkage on the surface of *M. barkeri* under light irradiation (Fig. S5). Meanwhile, the stagnation of the CO₂-to-CH₄ conversion and almost unchanged *mcrA* gene copies in *M. barkeri*-CdS biohybrid (dark) group suggested the necessity of a light-driven methanogenesis behavior of the *M. barkeri*-CdS biohybrid. Although the positive effects of hybrid CdS catalysts on the CO₂-to-CH₄ conversion have been reported such as TiO₂/CdS, TiO₂-supported Pt@CdS core-shell nanoparticles, and g-C3N4/CdS photocatalysts [28–30], the bare CdS (or *M. barkeri* (dead)-CdS in the present study) did not realize CH₄ production under light irradiation. The possible reasons might be attributed to the rapid recombination of photogenerated electrons and holes on bare CdS [31], which limited the photoelectrons transfer and utilization for CO₂ reduction to CH₄. In addition, the conduction band of the prepared CdS was also negative enough for the reduction of protons to H₂ (2H⁺ + 2e[−] → H₂, E⁰ = −0.42 V vs NHE at pH = 7), which could compete for the photoelectrons with the CO₂ reduction to CH₄. Due to the low reactivity of CO₂ molecules in chemical transformations and the absence of highly selective sites in bare CdS, H₂ would become the main photocatalytic products [32]. Therefore, only a small amount of H₂ (1.46 ± 0.01 μmol) was detected in the bare CdS group, and this was consistent with previous research [33]. To further confirm the CH₄ source, the isotopic labeling experiments were conducted with ¹³C-labeled NaHCO₃ as the carbon source/electron acceptor. Only the peaks of ¹³CH₄ (*m/z* = 17) and ¹³CO₂ (*m/z* = 45) were detected, demonstrating that the produced CH₄ was derived from the CO₂ reduction (Fig. 3C).

As shown in Fig. 3A, the CH₄ production by *M. barkeri*-CdS biohybrid began to plateau after 72 h of irradiation. Considering the sufficient CO₂ in the headspace (Fig. 3C) and the increasing concentration of sulfur over time (data no shown), we speculated that the possible reason might be related to the quick depletion of only sacrificial hole scavenger Cys, resulting in the photooxidative dissolution of CdS [34] and then the oxidative photodamage of cells [22]. To further confirm this speculation, a second injection of Cys in varying amounts (0.10, 0.20, 0.30 wt%) was conducted after 48 h of irradiation. The results showed that the CH₄ yield was increased with the increasing amount of Cys after the additional 72 h of photosynthesis (Fig. S6). Therefore, the cease of the CH₄ production in *M. barkeri*-CdS biohybrid could be attributed to the depletion of sacrificial hole scavenger Cys that quenched the photogenerated holes to suppress the recombination of photo-induced charge carriers (2Cys + 2h⁺ → Cyss + 2H⁺).

To mimic the day-night cycles, the light-dark cycle of 12 h was employed to investigate the photosynthetic behavior of the *M. barkeri*-CdS biohybrid. As shown in Fig. 3D, the CO₂ reduction rate reached 0.28–0.36 μmol/h in the light cycle with the *M. barkeri*-CdS biohybrid during the first two light-dark cycles. Unexpectedly, the CH₄ concentration continued to increase in the dark cycles with the CO₂ reduction rate of 0.07–0.15 μmol/h. The NADH/NAD ratio test showed higher intracellular reduction potential of *M. barkeri*-CdS biohybrid under light irradiation (Fig. S7), indicating that the photogenerated electrons could trigger the quicker recycling of NADH inside the cell. This was beneficial for biological CO₂ reduction in the dark cycle because the accumulated NADH could act as the additional electron donors.

The highest QE of 0.34% with a CH₄ production rate of 0.19 μmol/h was achieved at the light intensity of 1.07 ± 0.14 mW/cm² (Fig. S8). This QE value was comparable to that of plants or algae (0.2–1.6%) [22]. A higher light intensity resulted in the decreased QE, possibly due to the photooxidative degradation of CdS under a high light intensity that might cause the destruction of the cell membrane [35,36]. Meanwhile, the higher light intensity could also inactivate some functional proteins of *M. barkeri* that might take part in the photoelectron transfer process [37].

3.3. Proposed e[−] transfer mechanism of the *M. barkeri*-CdS biohybrid

Membrane-associated proteins have been demonstrated to take part

in the energy-conserving electron transport chain of cytochrome-containing methanogens during the CO₂-to-CH₄ conversion [7]. To understand the role of membrane-bound proteins of *M. Barkeri* in the photoelectron transfer of the *M. barkeri*-CdS biohybrid, different doses (1.0, 2.5, 5.0 U/mL) of proteinase K were used to digest the membrane-bound protein before the combination with CdS nanoparticles. Flow cytometry measurement showed that at the highest dose of 5.0 U/mL, less than 2.21% of the cells were damaged after the proteinase K treatment (Fig. 4A, B, Fig. S9), in accordance with the LIVE-DEAD staining image using the confocal laser scanning microscopy (CLSM) (Fig. 4C, D). Those results suggested that the vitality of *M. barkeri* was not significantly influenced by the proteinase K treatment. However, the *M. barkeri* (proteinase K treatment)-CdS biohybrid gradually lost the ability to produce CH₄ with the increasing dose of proteinase K (Fig. 4E), indicating the predominant role of membrane-bound proteins in the CO₂-to-CH₄ conversion.

Ferredoxin-dependent (Ech) hydrogenase was the distinct type of membrane-bound enzyme of *M. barkeri*, and consisted of four hydrophilic and two hydrophobic subunits, corresponding to EchA-F operon [38]. Quantitative RT-PCR experiments showed that the transcript levels of Ech hydrogenase were increased under light irradiation (Fig. 4F), indicating the potential role of Ech hydrogenase in energy-conserving electron transport in the *M. barkeri*-CdS biohybrid. This might be related to that a large quantity of photogenerated e[−] could be used to catalyze the reversible reduction of ferredoxin (driven by *EchF*), which involved the first step of methanogenesis for reduction of CO₂ to formyl-methanofuran (CHO-MFR). In addition, the photogenerated e[−] could be transferred through NiFe active sites in *EchE* for H₂ production as a crucial intermediate [39]. Then, the produced intracellular H₂ could be not only used as electron donors for ferredoxin reduction, but also be captured and oxidized by the methanophenazine-dependent (Vht) hydrogenase, particularly *VhtA* gene, demonstrating by its increasing transcript level (1.3 ± 0.1 fold). Therefore, the higher H₂ase expression (Ech and Vht) under light irradiation suggested the possible H₂ase-mediated electron transfer pathway in the *M. barkeri*-CdS biohybrid. The results were consistent with the previous studies, in which the direct electron transfer between metal chalcogenide nanoparticles and purified H₂ases in vitro was demonstrated [40,41]. Meanwhile, *VhtC* and *HdrE* were the important membrane-bound cytochrome *b* in *M. barkeri*. It was demonstrated that the photoelectrons could be injected to the membrane-bound cytochromes [42,43]. Thus, we predicted that photoelectrons from CdS nanoparticles could directly pass from *VhtC* and *HdrE* to the terminal electron acceptors that took part in the reduction of CoM-S-S-CoB. The significantly increasing transcript levels of *VhtC* (1.5 ± 0.1 fold) and *HdrE* (2.0 ± 0.2 fold) under light irradiation has demonstrated that cytochrome-mediated mechanism was also an important functional photoelectron transfer pathway in the *M. barkeri*-CdS biohybrid.

A proposed photoelectrons transfer mechanism in the *M. barkeri*-CdS biohybrid is shown in Fig. 5. The photoelectrons from the e[−]-h⁺ separation under light irradiation in CdS nanoparticles could be injected to the out-membrane proteins of *M. barkeri*, which is then used for the CO₂-to-CH₄ reduction. Among different types of out-membrane proteins, membrane-associated H₂ases such as Ech and Vht can be a candidate electron acceptor. In addition, non-H₂ases-mediated pathway might also be involved in the charge and energy transfer in the present biohybrid. For instance, the conduction band e[−] could be transferred to membrane-bound cytochromes. Understanding and identification of the novel and highly functional electron transfer pathways in the *M. Barkeri*-CdS biohybrid warrants further investigation.

4. Conclusions

We have successfully demonstrated the light-driven conversion of CO₂ to CH₄ by combination of CdS nanoparticles with *M. barkeri*. This *M. barkeri*-CdS biohybrid achieved a CH₄ production rate of 0.19 μmol/

h with a quantum efficiency of 0.34%. The increase of *mcrA* gene copies and the continuous CO₂ reduction in the dark periods during the simulated day-night cycles illustrated the robustness of the *M. barkeri*-CdS biohybrid for light harvesting. Membrane-bound proteins such as H₂ases and cytochromes were found to play a key role in the photo-electron transfer in the *M. barkeri*-CdS biohybrid. The findings can have important implications to developing semi-artificial photosynthesis for CO₂ conversion through exploring interactions between novel nano-photoconductors and microorganisms.

Declarations of interest

None.

Acknowledgments

This work was supported by the National Natural Science Foundation of China (51608121, 41671264 and 91751109), the National Key Research and Development Program of China (2017YFD0800900), the Project of Fujian Provincial Department of Science and Technology of China (2018J01748), the Fujian Agriculture and Forestry University Program for Distinguished Young Scholar (No. XJQ2017003), and US National Science Foundation (1603190).

Appendix A. Supplementary data

Supplementary material related to this article can be found, in the online version, at doi:<https://doi.org/10.1016/j.apcatb.2019.117916>.

References

- [1] T.R. Anderson, E. Hawkins, P.D. Jones, CO₂, the greenhouse effect and global warming: from the pioneering work of Arrhenius and Callendar to today's Earth System Models, *Endeavour* 40 (2016) 178–187.
- [2] C. Costentin, M. Robert, J.M. Saveant, Catalysis of the electrochemical reduction of carbon dioxide, *Chem. Soc. Rev.* 42 (2013) 2423–2436.
- [3] C.S. Diercks, Y. Liu, K.E. Cordova, O.M. Yaghi, The role of reticular chemistry in the design of CO₂ reduction catalysts, *Nat. Mater.* 17 (2018) 301–307.
- [4] S. Back, Y. Jung, TiC- and TiN-supported single-atom catalysts for dramatic improvements in CO₂ electrochemical reduction to CH₄, *ACS Energy Lett.* 2 (2017) 969–975.
- [5] E.M. Nichols, J.J. Gallagher, C. Liu, Y. Su, J. Resasco, Y. Yu, Y. Sun, P. Yang, M.C. Chang, C.J. Chang, Hybrid bioinorganic approach to solar-to-chemical conversion, *Proc. Natl. Acad. Sci. U. S. A.* 112 (2015) 11461–11466.
- [6] W. Tristan, E. Ulrich, S. Seigo, The methanogenic CO₂ reducing-and-fixing enzyme is bifunctional and contains 46 [4Fe-4S] clusters, *Science* 354 (2016) 114.
- [7] L. Shi, H. Dong, G. Reguera, H. Beyenal, A. Lu, J. Liu, H.Q. Yu, J.K. Fredrickson, Extracellular electron transfer mechanisms between microorganisms and minerals, *Nat. Rev. Microbiol.* 14 (2016) 651–662.
- [8] Z. Jiang, B. Wang, J.C. Yu, J. Wang, T. An, H. Zhao, H. Li, S. Yuan, P.K. Wong, AgInS₂/In₂S₃ heterostructure sensitization of *Escherichia coli* for sustainable hydrogen production, *Nano Energy* 46 (2018) 234–240.
- [9] N. Kornienko, J.Z. Zhang, K.K. Sakimoto, P. Yang, E. Reisner, Interfacing nature's catalytic machinery with synthetic materials for semi-artificial photosynthesis, *Nat. Nanotechnol.* 13 (2018) 890–899.
- [10] L. Xu, Y. Zhao, K.A. Owusu, Z. Zhuang, Q. Liu, Z. Wang, Z. Li, L. Mai, Recent advances in nanowire-biosystem interfaces: from chemical conversion, energy production to electrophysiology, *Chemistry* 4 (2018) 1538–1559.
- [11] M. Kumar, P.C. Sahoo, S. Srikanth, R. Bagai, S.K. Puri, S.S.V. Ramakumar, Photosensitization of electro-active microbes for solar assisted carbon dioxide transformation, *Bioresour. Technol.* 272 (2019) 300–307.
- [12] S. Cheng, D. Xing, D.F. Call, B.E. Logan, Direct biological conversion of electrical current into methane by electromethanogenesis, *Environ. Sci. Technol.* 43 (2009) 3953–3958.
- [13] M. Kouhnnavard, S. Ikeda, N.A. Ludin, N.B. Ahmad Khairudin, B.V. Ghaffari, M.A. Mat-Teridi, M.A. Ibrahim, S. Sepeai, K. Sopian, A review of semiconductor materials as sensitizers for quantum dot-sensitized solar cells, *Renew. Sust. Energy Rev.* 37 (2014) 397–407.
- [14] B. Wang, C. Zeng, K.H. Chu, D. Wu, H.Y. Yip, L. Ye, P.K. Wong, Enhanced biological hydrogen production from *Escherichia coli* with surface precipitated cadmium sulfide nanoparticles, *Adv. Energy Mater.* 7 (2017) 1700611.
- [15] W. Cai, W. Liu, Z. Zhang, K. Feng, G. Ren, C. Pu, H. Sun, J. Li, Y. Deng, A. Wang, *mcrA* sequencing reveals the role of basophilic methanogens in a cathodic methanogenic community, *Water Res.* 136 (2018) 192–199.
- [16] D. Yuan, L. Zhang, J. Lai, L. Xie, B. Mao, D. Zhan, SECM evaluations of the crystal-facet-correlated photocatalytic activity of hematites for water splitting, *Electrochim. Commun.* 73 (2016) 29–32.
- [17] J. Heise, M. Nega, M. Alawi, D. Wagner, Propidium monoazide treatment to distinguish between live and dead methanogens in pure cultures and environmental samples, *J. Microbiol. Meth.* 121 (2016) 11–23.
- [18] J. Ye, A. Hu, G. Ren, T. Zhou, G. Zhang, S. Zhou, Red mud enhances methanogenesis with the simultaneous improvement of hydrolysis-acidification and electrical conductivity, *Bioresour. Technol.* 247 (2018) 131–137.
- [19] F. Vaquero, R.M. Navarro, J.L.G. Fierro, Influence of the solvent on the structure, morphology and performance for H₂ evolution of CdS photocatalysts prepared by solvothermal method, *Appl. Catal. B-Environ.* 203 (2017) 753–767.
- [20] J. Yu, Y. Yu, P. Zhou, W. Xiao, B. Cheng, Morphology-dependent photocatalytic H₂-production activity of CdS, *Appl. Catal. B-Environ.* 156–157 (2014) 184–191.
- [21] T. Di, B. Zhu, J. Zhang, B. Cheng, J. Yu, Enhanced photocatalytic H₂ production on CdS nanorod using cobalt-phosphate as oxidation cocatalyst, *Appl. Surf. Sci.* 389 (2016) 775–782.
- [22] K.K. Sakimoto, A.B. Wong, P. Yang, Self-photosensitization of nonphotosynthetic bacteria for solar-to-chemical production, *Science* 351 (2016) 74–77.
- [23] R. Vogel, P. Hoyer, H. Weller, Quantum-sized PbS, CdS, Ag₂S, Sb₂S₃, and Bi₂S₃ particles as sensitizers for various nanoporous wide-bandgap semiconductors, *J. Phys. Chem.* 98 (1994) 3183–3188.
- [24] J. Low, B. Cheng, J. Yu, Surface modification and enhanced photocatalytic CO₂ reduction performance of TiO₂: a review, *Appl. Surf. Sci.* 392 (2017) 658–686.
- [25] A.J. Stams, C.M. Plugge, Electron transfer in syntrophic communities of anaerobic bacteria and archaea, *Nat. Rev. Microbiol.* 7 (2009) 568–577.
- [26] R. Morris, A. Schauer-Gimenez, U. Bhattachar, C. Kearney, C.A. Struble, D. Zitomer, J.S. Maki, Methyl coenzyme M reductase (*mcrA*) gene abundance correlates with activity measurements of methanogenic H₂/CO₂-enriched anaerobic biomass, *Microb. Biotechnol.* 7 (2014) 77–84.
- [27] K.D. Olson, C.W. McMahon, R.S. Wolfe, Light sensitivity of methanogenic archaeabacteria, *Appl. Environ. Microb.* 57 (1991) 2683–2686.
- [28] Hyunwoong Park, Hsin-Hung Ou, Unseock Kang, Jina Choi, R. Hoffmann Michael, Photocatalytic conversion of carbon dioxide to methane on TiO₂/CdS in aqueous isopropanol solution, *Catal. Today* 266 (2016) 153–159.
- [29] Y. Wei, J. Jiao, Z. Zhao, W. Zhong, J. Li, J. Liu, G. Jiang, A. Duan, 3D ordered macroporous TiO₂-supported Pt@CdS core-shell nanoparticles: design, synthesis and efficient photocatalytic conversion of CO₂ with water to methane, *J. Mater. Chem. A* 3 (2015) 11074–11085.
- [30] W.J. Ong, L.L. Tan, S.P. Chai, S.T. Yong, A.R. Mohamed, Surface charge modification via protonation of graphitic carbon nitride (g-C₃N₄) for electrostatic self-assembly construction of 2D/2D reduced graphene oxide (rGO)/g-C₃N₄ nanostructures toward enhanced photocatalytic reduction of carbon dioxide to methane, *Nano Energy* 13 (2015) 757–770.
- [31] J. Ran, J. Yu, M. Jaroniec, Ni(OH)₂ modified CdS nanorods for highly efficient visible-light-driven photocatalytic H₂ generation, *Green Chem.* 13 (2011) 2708–2713.
- [32] R. Long, Y. Li, Y. Liu, S. Chen, X. Zheng, C. Gao, C. He, N. Chen, Z. Qi, S. Li, J. Jiang, J. Zhu, Y. Xiong, Isolation of Cu atoms in Pd lattice: forming highly selective sites for photocatalytic conversion of CO₂ to CH₄, *J. Am. Chem. Soc.* 139 (2017) 4486–4492.
- [33] J. Wang, T. Xia, L. Wang, X. Zheng, Z. Qi, C. Gao, J. Zhu, Z. Li, H. Xu, Y. Xiong, Enabling visible-light-driven selective CO₂ reduction by doping quantum dots: trapping electrons and suppressing H₂ evolution, *Angew. Chem. Int. Ed.* 57 (2018) 16447–16451.
- [34] M. Chen, X.F. Zhou, Y.Q. Yu, X. Liu, R.J.X. Zeng, S.G. Zhou, Z. He, Light-driven nitrous oxide production via autotrophic denitrification by self-photosensitized *Thiobacillus denitrificans*, *Environ. Int.* 127 (2019) 353–360.
- [35] L.M. Paulo, A.J. Stams, D.Z. Sousa, Methanogens, sulphate and heavy metals: a complex system, *Rev. Environ. Sci. Bio* 14 (2015) 537–553.
- [36] Z. Qin, Q. Yue, Y. Liang, J. Zhang, L. Zhou, O.B. Hidalgo, X. Liu, Extracellular biosynthesis of biocompatible cadmium sulfide quantum dots using *Trametes versicolor*, *J. Biotechnol.* 284 (2018) 52–56.
- [37] K.A. Brown, M.B. Wilker, M. Boehm, G. Dukovic, P.W. King, Characterization of photochemical processes for H₂ production by CdS nanorod-[FeFe] hydrogenase complexes, *J. Am. Chem. Soc.* 134 (2012) 5627–5636.
- [38] T.D. Mand, G. Kulkarni, W.W. Metcalf, Genetic, biochemical, and molecular characterization of *Methanosaerica barkeri* mutants lacking three distinct classes of hydrogenase, *J. Bacteriol.* 200 (2018) e00342–18.
- [39] S. Morra, F. Valetti, S.J. Sadeghi, P.W. King, T. Meyer, G. Gilardi, Direct electrochemistry of an [FeFe]-hydrogenase on a TiO₂ Electrode, *Chem. Commun.* 47 (2011) 10566–10568.
- [40] J.K. Utterback, M.B. Wilker, K.A. Brown, P.W. King, J.D. Eaves, G. Dukovic, Competition between electron transfer, trapping, and recombination in CdS nanorod-hydrogenase complexes, *Phys. Chem. Chem. Phys.* 17 (2015) 5538–5542.
- [41] M.B. Wilker, K.E. Shinopoulos, K.A. Brown, D.W. Mulder, P.W. King, G. Dukovic, Electron transfer kinetics in CdS nanorod-[FeFe]-hydrogenase complexes and implications for photochemical H₂ generation, *J. Am. Chem. Soc.* 136 (2014) 4316–4324.
- [42] N. Kornienko, K.K. Sakimoto, D.M. Herlihy, S.C. Nguyen, P. Yang, Spectroscopic elucidation of energy transfer in hybrid inorganic-biological organisms for solar-to-chemical production, *Proc. Natl. Acad. Sci. U. S. A.* 113 (2016) 11750–11755.
- [43] J. Ye, A. Hu, G. Ren, M. Chen, J. Tang, P. Zhang, S. Zhou, Z. He, Enhancing sludge methanogenesis with improved redox activity of extracellular polymeric substances by hematite in red mud, *Water Res.* 134 (2018) 54–62.